JOURNAL OF MATERIALS SCIENCE 17 (1982) 3598–3610

Dissolution kinetics of MgO crystals in aqueous acidic salt solutions

K. SANGWAL
Institute of Physics, Technical University of Łódź, Wólczańska 219, 93005 Łódź, Poland

The revelation and morphology of dislocation etch pits as well as the rates of macroscopic dissolution and selective etching on the {1 0 0} plane of MgO crystals in aqueous solutions of various inorganic salts are investigated in relation to the nature and concentration of salt in solution and the etching temperature. It is found that addition of a salt generally facilitates etch pit formation and that the rates of surface dissolution and selective etching increase with additive concentration, etchant temperature and character and ageing of dislocations, while the etch pit morphology depends on the concentration and chemical nature of an impurity, etching temperature and the ageing of the dislocations. It is also observed that some fast etching solutions produce very shallow etch pits at screw dislocations. The results are discussed from a consideration of solution pH, standard electrode potentials of metals and stability of complexes present in solution. The importance of the surface entropy factor in revealing etch pits at screw dislocations is pointed out.

1. Introduction

Three types of theory explain the formation of etch pits at dislocation sites. In the topochemical theories, dislocations are considered as centres of relatively more adsorption activity by virtue of a higher adsorption potential which ensures a higher reaction rate at them [1]. The thermodynamic theories assume that the activation energy for pit nucleation at a dislocation site is smaller than that on a perfect surface because of the elastic strain [2, 3] or core energy of the dislocation [4, 5]. Topochemical adsorption and thermodynamic mechanisms of dislocation etch pit formation are essentially two-dimensional nucleation mechanisms. The spiral mechanism of etch pit formation is exactly the reverse of crystal growth in the presence of a screw dislocation [2, 6–8], where the dislocation provides a continuous source of dissolution steps. For geometrical reasons edge dislocations are not expected to produce etch pits by this mechanism.

It is known [9–12] that aqueous solutions of acids and acidic salts are reliable dislocation etchants for MgO crystals, and that the morphology of dislocation etch pits changes with the concentration of the etchant. It is also found [11, 13, 14] that the rates of macroscopic dissolution and lateral growth of etch pits depend on the etchant concentration and temperature. These results were interpreted from a consideration of the dissociation of an acid into anions and cations and their subsequent reaction with the crystal through an activated complex [1].

Many etchants differentiate between edge and screw, and between fresh and aged dislocations emerging on {1 0 0} and {1 1 0} faces of MgO crystals [13]. Such observations have also been recorded on NaCl [15], LiF [16], $BaSO_4$ [17], $CaWO_4$ [18] and natrolyte crystals [19]. In fact in some cases spiral etch pits are produced at the sites of screw dislocations [20–23]. The difference between edge and screw dislocation etch pits and the formation of spiral etch pits is observed only when the etchant composition and temperature are properly selected. However, while the overwhelming majority of experimental data on etch pit formation appears to be consistent with the two-dimensional nucleation mechanisms, these observations indicate that pits do form by the spiral mechanism.

During an analysis of the experimental data on etch pit formation, it was concluded that solvents,

0022–2461/82/123598–13$04.06/0

in which a crystal is more soluble, are better selective etchants [24–26] and that not only additive salts but reaction products can also lead to the formation of contrasting dislocation etch pits [25]. Formally, the solubility criterion means that with an increase in solubility the rate of nucleation along the dislocation line is increased, while the second criterion implies that either the rate of nucleation along the dislocation line is increased or the rate of lateral growth of pits is retarded.

Inorganic salts in aqueous solutions exist in the form of *aquo* entities whose chemical constitution depends on salt concentration and solution temperature [27–31]. Also, there are many salts which are acidic in nature. The acidity of an aqueous solution of acidic salts increases with the salt concentration. Consequently, during etching, an acidic salt in aqueous solution provides *aquo* complexes as well as an acidic medium. Therefore, investigation of etching kinetics in aqueous solutions of acidic salts should clarify the influence of solubility and complex species present in solution on etch pit formation on crystal surfaces.

In the present paper the results of an investigation of the kinetics of macroscopic dissolution and selective etching and of the etch patterns formed on the {1 0 0} surface of MgO crystals in aqueous solutions of chlorides of bi- and trivalent cations are presented and discussed.

2. Experimental procedure

Specimens with {1 0 0} planes were prepared by cleavage in the form of rectangular parallelopipeds with dimensions less than 11 mm × 4 mm × 4 mm from a large MgO crystal. Before being etched, they were polished in 44.1 N H_3PO_4 at 100 to 110° C. Etching was carried out by placing them in 150 cm^3 beakers containing 80–100 cm^3 of etching solution at constant temperature. After particular durations, the samples were extracted from the beakers, rinsed in water and dried with filter paper. The rate of macroscopic dissolution, v_d, was calculated from the loss in weight of the samples by dissolution after a particular time, while the rate of apparent lateral growth, v'_t, of fresh dislocation etch pits was computed from their size. The rate of apparent normal etching, v'_n, along the dislocation line was estimated by focusing the microscope at the pit apex and at the surface around it. For larger pits, with a depth of about 7 μm, the rates were reproducible within ± 6%, but for smaller pits the variation was up to ± 15%. Hence, to reduce the errors in depth measurements, the samples were invariably etched for sufficiently long durations. The method adopted to estimate v_d and v'_t has been described earlier [14].

The salts selected for preparing the etching solutions were chlorides of bi- and trivalent cations. They were selected for the following reasons:

(1) They produce etch pits on the {1 0 0} face of MgO crystals.

(2) Most of them are soluble in water.

(3) The chemical constitution of the aqueous complexes present in aqueous solutions of chlorides, as studied by ultraviolet–visible spectra, is known.

The rates of true lateral growth, v_t, and true normal etching along the dislocation line, v_n, are related to the apparent rates v'_t and v'_n by the relations

$$v_t = v'_t(1 + v_d/v'_n), \quad (1)$$

$$v_n = v'_n + v_d. \quad (2)$$

From the experimental values of v_d, v'_t and v'_n, v_t and v_n were computed. The values of v_d (in g cm^{-2} h^{-1}) calculated experimentally were converted into cm h^{-1} units by dividing them by the density of MgO, $\rho = 3.58$ g cm^{-3}.

The ultraviolet–visible absorption and transmission spectra of $FeCl_3 \cdot 6H_2O$ and $CuCl_2 \cdot 2H_2O$ aqueous solutions were recorded using a Carl Zeiss Specord spectrophotometer, while the pH of the solutions was determined employing an OP-211-type pH meter (Hungary). The precipitated reaction products remaining in the beakers after etching the samples were identified by usual chemical tests.

3. Experimental results

3.1. Effect of $CuCl_2 \cdot 2H_2O$ and $FeCl_3 \cdot 6H_2O$ concentration on pH of solutions

The dependence of solution pH on salt concentration is illustrated in Fig. 1. It may be noted from the figure that above about 10^{-1} M $FeCl_3 \cdot 6H_2O$ and 10^{-2} M $CuCl_2 \cdot 2H_2O$ the pH rapidly decreases with salt concentration, but below these concentrations the pH decreases relatively slowly. By extrapolating the curves to the pH axis it may be seen that at $CuCl_2 \cdot 2H_2O$ concentration of about 10^{-6} M the pH corresponds to that of pure water,

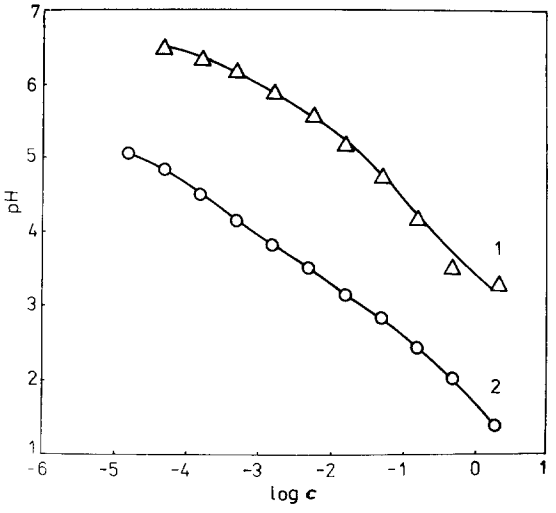

Figure 1 Graph showing the dependence of solution pH on the concentration of (1) $CuCl_2 \cdot 2H_2O$ and (2) $FeCl_3 \cdot 6H_2O$.

but in the case of $FeCl_3 \cdot 6H_2O$ the concentration is of the order of 10^{-10} M.

3.2. Chemical constitution of complexes in solutions of $CuCl_2 \cdot 2H_2O$ and $FeCl_3 \cdot 6H_2O$

The positions of peaks of absorption and transmission spectra for solutions of various concentrations of $CuCl_2 \cdot 2H_2O$ and $FeCl_3 \cdot 6H_2O$ are listed in Table I. The constitutions of the possible complexes, as inferred from the literature values of peaks [30, 31], corresponding to the salt concentrations, are also included in the table. At concentrations below 10^{-3} M of $CuCl_2 \cdot 2H_2O$ and 5×10^{-5} M of $FeCl_3 \cdot 6H_2O$, pure *aquo* complexes (i.e. $[Cu(H_2O)_6]^{2+}$ and $[Fe(H_2O)_6]^{3+}$, respectively) are formed; above these concentrations chlorine-substituted *aquo* and *nonaquo* complexes are formed.

3.3. Composition of reaction products formed during etching

The reaction products formed during the etching of MgO in solutions of $CuCl_2 \cdot 2H_2O$ and $FeCl_3 \cdot 6H_2O$ are insoluble whitish blue and dark brown precipitates, respectively. Usual wet tests used in inorganic chemical analysis indicated that the precipitates correspond to $Cu(OH)_2$ and $Fe(OH)_3$.

3.4. Effect of salt concentration and solution temperature on the morphology of dislocation etch pits

The etch-pit pattern produced by distilled water is shown in Fig. 2, while the etch-pit patterns formed by $CuCl_2 \cdot 2H_2O$ and $FeCl_3 \cdot 6H_2O$ in their aqueous solutions at different concentrations are displayed in Figs 3 and 4, respectively. It may be noted that H_2O forms sharp, contrasting ⟨1 0 0⟩ pits at edge and screw dislocations. In $CuCl_2 \cdot 2H_2O$, with an increase in its concentration, the pits acquire a sharp octagonal morphology. With an increase in the salt concentration the edge dislocation etch pits remain contrasting but screw dislocation pits

TABLE I Positions of peaks of ultraviolet–visible spectra of aqueous solutions of $FeCl_3 \cdot 6H_2O$ and $CuCl_2 \cdot 2H_2O$, and complexes at different salt concentrations

Salt concentration (M)	Peak positions (nm)		Complex
	Transmission	Absorption	
$FeCl_3 \cdot 6H_2O$			
2.5–5 $\times 10^{-1}$	630, 200–450*	NI†	$[FeCl_3]_n$
1 –5 $\times 10^{-2}$	500, 200–370*	250–400	$[FeCl_4]^-$
2 $\times 10^{-3}$	200–335*	NI	$[FeCl_3(H_2O)_3]$
2×10^{-4}–1 $\times 10^{-3}$	295	230, 295	$[FeCl_2(H_2O)_4]^+$
1 $\times 10^{-4}$	280	NI	$[FeCl(H_2O)_5]^{2+}$
5 $\times 10^{-5}$	220, 275	215, 260–270	$[FeCl(H_2O)_5]^{2+}$, $[Fe(H_2O)_6]^{3+}$
2.5 $\times 10^{-5}$	220	NI	$[Fe(H_2O)_6]^{3+}$
$CuCl_2 \cdot 2H_2O$			
5 $\times 10^{-2}$	< 275, > 800	280	$[CuCl_2]_n$
2.5 $\times 10^{-2}$	< 260	250	$[CuCl_4]^{2-}$
1 $\times 10^{-2}$	< 230, 255	230	$[CuCl(H_2O)_5]^+$
2.5–5 $\times 10^{-3}$	< 220	NI	$[CuCl(H_2O)_5]^+$, $[Cu(H_2O)_6]^{2+}$
1 $\times 10^{-3}$	205	210	$[Cu(H_2O)_6]^{2+}$

*A wide band is observed whose width increases with increasing salt concentration to higher wavelength side.
†NI means not investigated.

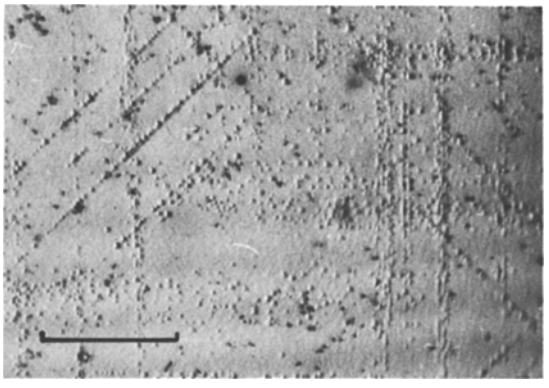

Figure 2 Etch-pit pattern produced on a {1 0 0} face of MgO by water at 24° C after 50 h. Scale bar = 30 μm.

become shallower. With an increase in $FeCl_3 \cdot 6H_2O$ concentration, ⟨1 0 0⟩, rounded octagonal, ⟨1 1 0⟩ and finally circular pits are formed in that order. In this case the pits formed at screw dislocations essentially maintain the same contrast. However, in both $FeCl_3 \cdot 6H_2O$ and $CuCl_2 \cdot 2H_2O$ the screw dislocation etch pits are always shallower and smaller than those formed at edge dislocations. Moreover, the pits formed at aged dislocations are always shallower and smaller than fresh dislocation etch pits. This behaviour of aged and fresh dislocations is analogous to that observed in several mineral acids [9, 12], but at very low concentrations $FeCl_3 \cdot 6H_2O$ simultaneously produces, even on the same face, three types of etch pits: ⟨1 0 0⟩ and octagonal etch pits at aged dislocations and ⟨1 1 0⟩ pits at fresh dislocations. Exactly similar observations have been made on CsI crystals [32].

The morphology of dislocation etch pits also changes with a change in solution temperature. With an increase in the temperature of an etchant containing a particular salt concentration, the pits acquire a morphology which corresponds to the one obtained at a lower impurity concentration. An example showing this feature for 0.5 M $CuCl_2 \cdot 2H_2O$ solution is illustrated in Fig. 5.

3.5. Effect of salt concentration and etchant temperature on etch rates

The dependence of macroscopic dissolution rate, v_d, apparent lateral etch rate, v'_t, and of apparent normal etch rate along the dislocation lines, v'_n, on

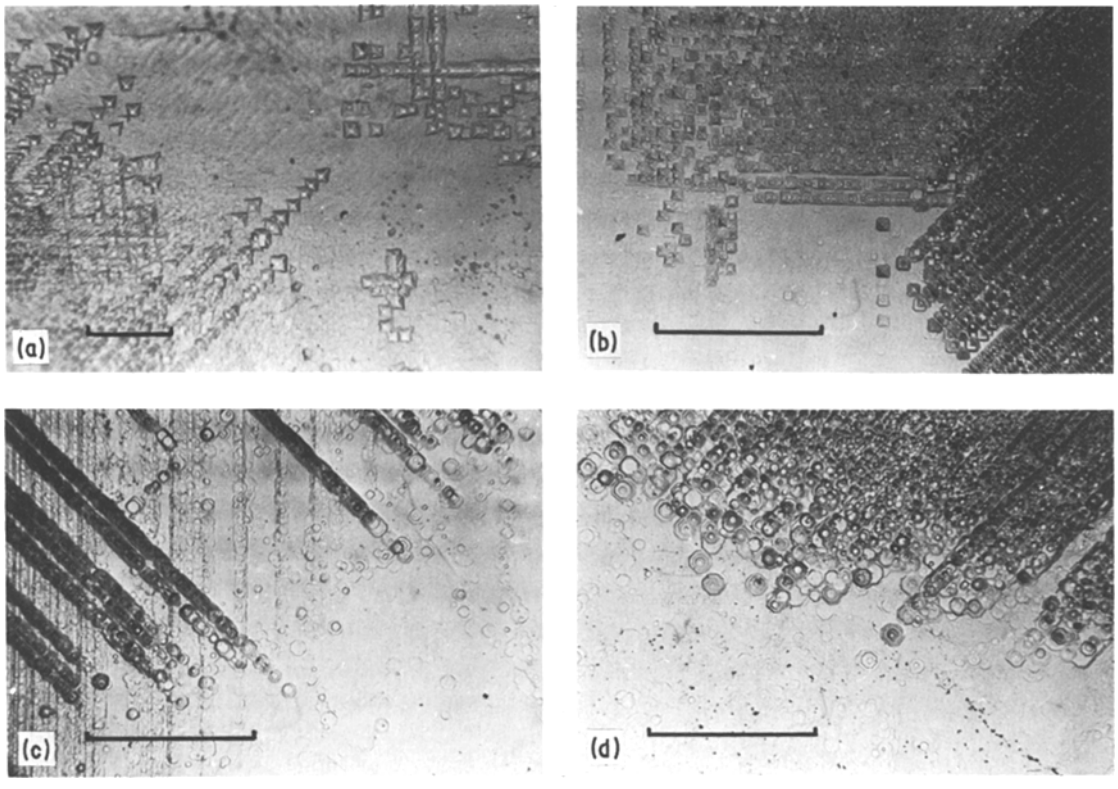

Figure 3 Etch pits produced on {1 0 0} face of MgO by etching in (a) 0.0167 M, (b) 0.167 M, (c) 0.5 M and (d) 2 M $CuCl_2 \cdot 2H_2O$ solutions at 21.2° C after etching for $21\frac{1}{3}$ h. Scale bar = 100 μm.

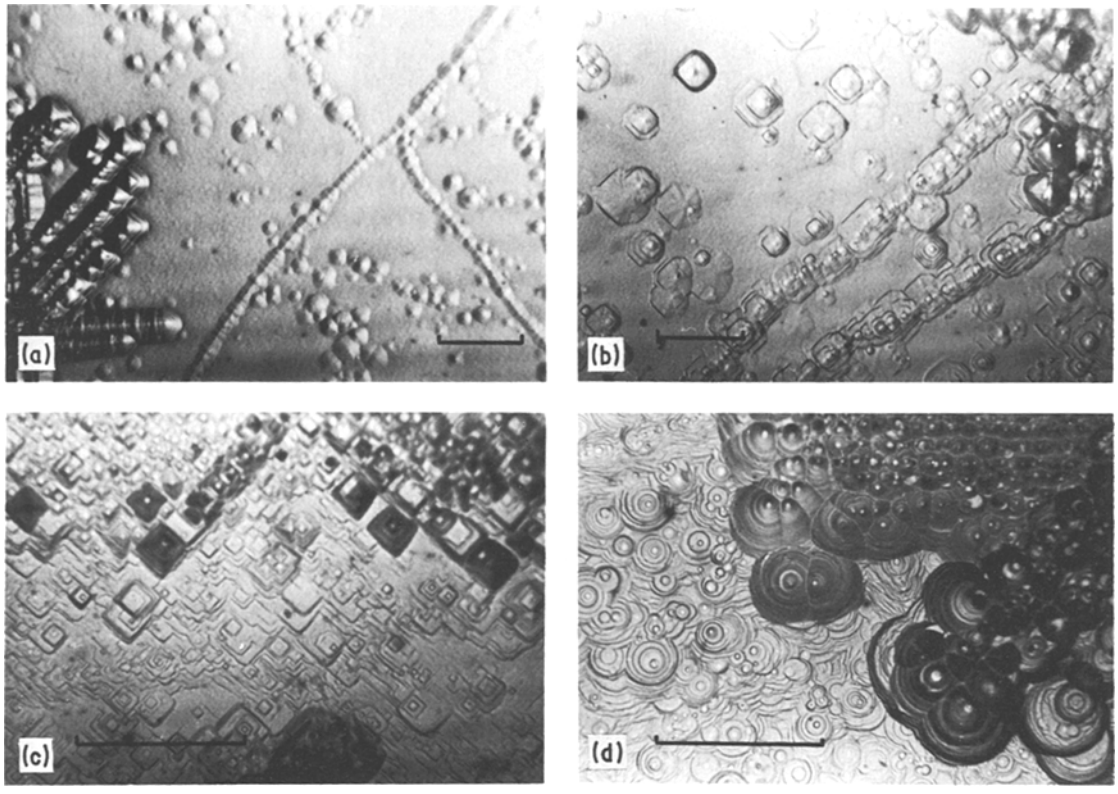

Figure 4 Etch patterns formed on {1 0 0} face by (a) 5×10^{-4} M, (b) 5×10^{-3} M, (c) 5×10^{-2} M and (d) 5×10^{-1} M $FeCl_3 \cdot 6H_2O$ solutions at 22° C after 18 h. Note pits with different morphologies in (a) and (b). Scale bar = 100 μm.

the concentration of $CuCl_2 \cdot 2H_2O$ and $FeCl_3 \cdot 6H_2O$ is shown in Figs 6 and 7, respectively. It may be noted from these figures that v_d and v_t' regularly increase with an increase in the salt concentration. The increase in v_d and v_t' with salt concentration is relatively poor above 5×10^{-4} M $FeCl_3 \cdot 6H_2O$ and above 10^{-1} M $CuCl_2 \cdot 2H_2O$, while a poor increase in v_t' with salt concentration starts at even much lower salt concentrations. With an increase in $FeCl_3 \cdot 6H_2O$ concentration the ratio v_n'/v_t' somewhat increases for both edge and screw dislocations, but at a particular concentration its value is always larger for edge dislocation etch pits (i.e. more contrasting pits are formed at edge dislocations than at screws). In the case of $CuCl_2 \cdot 2H_2O$, the etching behaviour of edge dislocations is similar to that observed in the case of $FeCl_3 \cdot 6H_2O$, but above about 10^{-2} M salt concentration the contrast of etch pits at screw dislocations regularly decreases. This etching behaviour of $CuCl_2 \cdot 2H_2O$ and $FeCl_3 \cdot 6H_2O$ may also be noted from Figs 3 and 4.

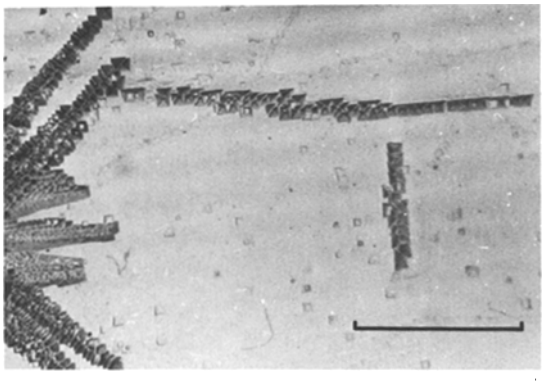

Figure 5 Etch pits produced by 5×10^{-1} M $CuCl_2 \cdot 2H_2O$ at 69.8° C after 25 min. Note the difference in the morphology of etch pits and contrast of screw dislocation pits seen in this figure and Fig. 3c. Scale bar = 200 μm.

The temperature dependence of etch pits for 0.5 M $FeCl_3 \cdot 6H_2O$ and $CuCl_2 \cdot 2H_2O$ solutions is illustrated in Figs 8 and 9, respectively. For $FeCl_3 \cdot 6H_2O$ each of the curves of the logarithm of apparent and true etch rates against inverse of absolute temperature can be approximated to the same straight line with a single activation energy and pre-exponential factor. However, for $CuCl_2 \cdot 2H_2O$, v_t' may be represented by a single

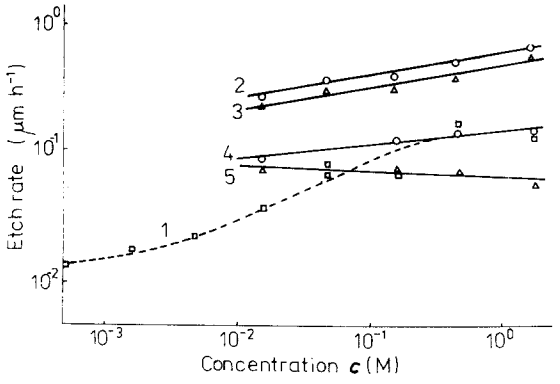

Figure 6 Dependence of etch rates on $CuCl_2 \cdot 2H_2O$ concentration at 21.2° C. (1) $-v_d$, (2) $-v'_{t,edge}$, (3) $-v'_{t,screw}$, (4) $-v'_{n,edge}$ and (5) $-v'_{n,screw}$.

line but v'_n has two slopes with different activation energies and pre-exponential factors. Obviously, the true v_t and v_n are also expected to show different slopes, as seen in Fig. 9. The estimated values of activation energies and pre-exponential factors for etching in the two solutions are listed in Table II.

3.6. Etching characteristics of various metal chloride solutions

The etching characteristics of 0.5 M solutions of various bi- and trivalent metal chloride salts* are summarized in Table III. The pH of the solutions, the standard electrode potentials of the respective metals [33], and the solubility and heat of formation of the metal hydroxides [33] are also included in the table. It may be noted from the table that among the salts used the fastest etchants for MgO are the solutions of trivalent metal

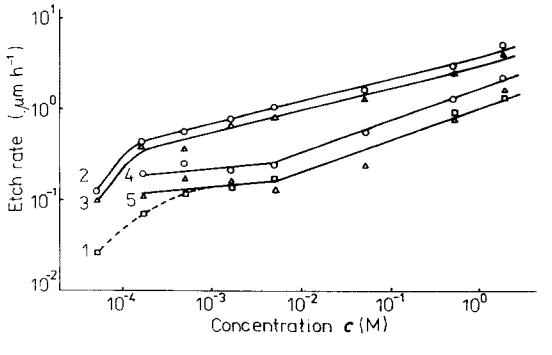

Figure 7 Dependence of etch rates on $FeCl_3 \cdot 6H_2O$ concentration at 22° C. (1) $-v_d$, (2) $-v'_{t,edge}$, (3) $-v'_{t,screw}$, (4) $-v'_{n,edge}$ and (5) $-v'_{n,screw}$.

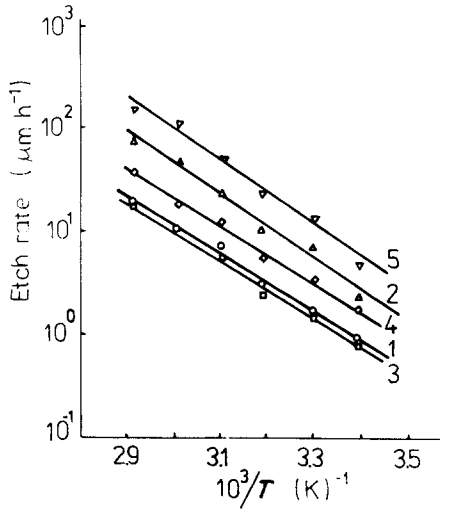

Figure 8 Temperature dependence of etch rates for 0.5 M $FeCl_3 \cdot 6H_2O$ solution: (1) $-v_d$, (2) $-v'_t$, (3) $-v'_n$, (4) $-v_t$ and (5) $-v_n$. v_t, v'_t, v_n and v'_n are computed for screw dislocations.

chlorides. Some typical photographs of the etch patterns produced by the above etchants are shown in Fig. 10.

4. Discussion

4.1. Dissolution rates and etch pit formation

With reference to Fig. 1, it may be noted that in

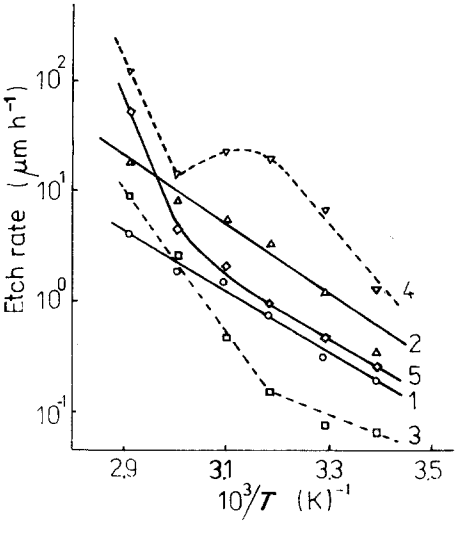

Figure 9 Temperature dependence of etch rates for 0.5 M $CuCl_2 \cdot 2H_2O$ solution: (1) $-v_d$, (2) $-v'_t$, (3) $-v'_n$, (4) $-v_t$ and (5) $-v_n$. The lateral and normal rates have been computed for screw dislocations.

*In $PbCl_2$, during etching the crystal surface is covered by a deposition which is insoluble in water but is removed by dilute acids. Therefore in the case of a saturated solution of $PbCl_2$, the etched surface was rinsed in formic acid.

TABLE II Activation energies and pre-exponential factors for etching of {1 0 0} surface of MgO crystals in 0.5 M $FeCl_3 \cdot 6H_2O$ and 0.5 M $CuCl_2 \cdot 2H_2O$ solutions

Additive salt	Macroscopic dissolution		Apparent selective etching				True selective etching			
	E_d(eV)	A_d(μm h^{-1})	E'_n(eV)	A'_n(μm h^{-1})	E'_t(eV)	A'_t(μm h^{-1})	E_n(eV)	A_n(μm h^{-1})	E_t(eV)	A_t(μm h^{-1})
$FeCl_3 \cdot 6H_2O$	0.56	2.8×10^9	0.56	2.5×10^9	0.62	9.4×10^{10}	0.56	5.3×10^9	0.62	2.0×10^{11}
$CuCl_2 \cdot 2H_2O$	0.54	3.1×10^8	0.37*	1.4×10^{6}*	0.62	2.2×10^{10}	0.54	4.2×10^8	1.08	3.8×10^{16}
			1.26	1.9×10^{20}			2.20†	3.7×10^{33}†	2.00†	4.3×10^{33}†

*Below and above 40° C.
†Above 60° C.

the concentration interval under study, the pH of the solution continuously decreases. However, the rate of decrease in pH is relatively more above the salt concentrations of 5×10^{-2} M $CuCl_2 \cdot 2H_2O$ and 5×10^{-4} M $FeCl_3 \cdot 6H_2O$. Since pH is connected with the dissociation of the salt, the relatively larger decrease in pH with salt concentration implies more dissociation of the salt. Consequently, the dissolution rate of MgO depends on the solution pH. Figs 6 and 7 clearly demonstrate this, but, corresponding to the same value of pH, a higher dissolution rate in $FeCl_3 \cdot 6H_2O$ than in $CuCl_2 \cdot 2H_2O$ indicates that other factors associated with the chemical nature of the salt also have an influence on its absolute value. The data presented in Table III also corroborate this inference.

Figs 6 and 7 show that above 5×10^{-2} M $CuCl_2 \cdot 2H_2O$ and 5×10^{-4} M $FeCl_3 \cdot 6H_2O$ concentrations, the increase in dissolution rate is relatively slow. Above these concentrations the complexes formed in solutions are negatively charged or molecular aggregates (Table I). These complexes are unfavourable for the dissolution of MgO (see Section 4.2). Further, the equilibrium constants of the substituted complexes, in general, are lower than those of the *aquo* entities [34]. Consequently, the effect of the nature of a salt on dissolution rates is more at lower concentrations. Therefore it may be argued that the stability of complexes also influences the dissolution rates.

The macroscopic dissolution rate is also affected by the standard electrode potential of the metal of an additive cation and its charge. Cations of more noble metals etch MgO at a faster rate (Table III). As seen from Table III, the solubility and heat of formation of the cation hydroxide do not influence the macroscopic dissolution rate.

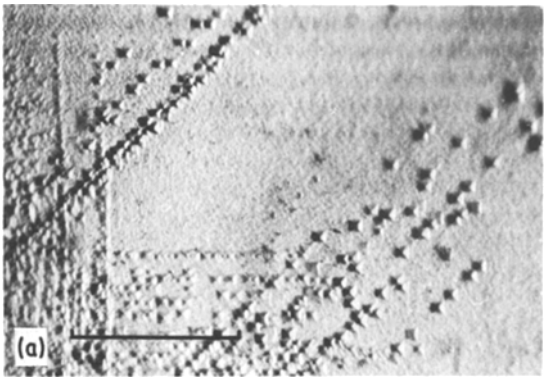

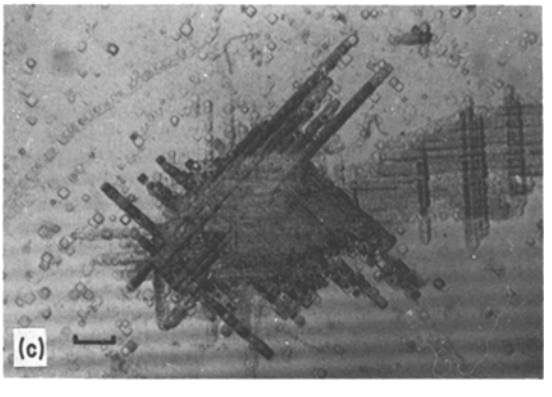

Figure 10 Etch patterns produced by (a) 0.5 M $NiCl_2$, (b) a saturated aqueous solution of $PbCl_2$ and (c) 0.5 M $AlCl_3 \cdot 6H_2O$ at 22.4° C. Etching time for (a) and (b) 20 h, and for (c) 5 h. Note the formation of sheaves and spherulites in (b). Scale bar = 40 μm.

TABLE III Etching characteristics of 0.5 M solutions of different metal chlorides at 22.4° C: solution pH, solubility and heat of formation, ΔH^0, of respective hydroxide; standard electrode potential of metal, E^0, at 25° C, and equilibrium constant K of salts

Added chloride of cation	v_d (μm h^{-1})	v'_t (μm h^{-1})	v'_n (μm h^{-1})	v'_t/v'_n	pH	E^0 (V)	α_J*	Hydroxide solubility (g per 100 cm^3 H_2O)	ΔH^0 (kcal mol^{-1})	log K	Remarks on pit orientation
†	1.7×10^{-3}	1.3×10^{-2}	‡	3–4	–	−2.34	5.82	9×10^{-4} (18)	−924.7	–	⟨1 0 0⟩ pits
Cu^{2+}	2.2×10^{-1}	4.0×10^{-1}	8.0×10^{-2}	5	3.50	+0.345	3.39	Insoluble	−448.5	2.80 (18)	Octagonal etch pits
Ni^{2+}	8.9×10^{-3}	8.8×10^{-2}	‡	3–4	5.95	−0.236	5.00	1.3×10^{-3} (cw) §	−538.1	–	⟨1 0 0⟩ pits
Co^{2+}	4.5×10^{-3}	4.4×10^{-2}	‡	3–4	3.87	−0.277	5.34	3.2×10^{-4} (cw)	−548.9	−2.40 (18)	⟨1 0 0⟩ pits
Pb^{2+}‖	2.8×10^{-2}	5.6×10^{-1}	9.0×10^{-2}	6.2	3.86	−0.126	4.42	1.55×10^{-2} (cw)	−514.6	1.10 (25)	Rounded ⟨1 1 0⟩ pits and overgrowths
Ba^{2+}	4.5×10^{-3}	1.1×10^{-1}	‡	3–4	5.02	−2.90	5.34	5.5 (15)	−946.4	−0.13	⟨1 0 0⟩ pits
Sr^{2+}	4.8×10^{-3}	1.5×10^{-2}	‡	3–4	6.36	−2.89	5.31	0.41 (0)	−959.4	–	Rounded ⟨1 1 0⟩ pits
Ca^{2+}	4.8×10^{-3}	–	–	–	6.86	−2.87	5.31	0.185 (0)	−986.6	–	No pits with surface becoming rough
Cd^{2+}	8.7×10^{-3}	3.9×10^{-2}	1.1×10^{-2}	3.5	4.70	−0.402	5.01	2.6×10^{-4} (25)	−557.6	1.39 (25)	⟨1 0 0⟩ pits and rounded ⟨1 1 0⟩ pyramidal hillocks
Zn^{2+}	9.5×10^{-3}	1.8×10^{-1}	5.0×10^{-2}	3.6	5.51	−0.736	4.96	Sparingly soluble	−642.2	−0.32 (25)	Octagonal etch pits with longer sides along ⟨1 0 0⟩
Al^{3+}	3.3×10^{-1}	1.26	3.0×10^{-1}	4.2	1.56	−1.67	3.19	Insoluble	–	–	⟨1 1 0⟩ pits
Fe^{3+}	1.1	2.4	8.5×10^{-1}	2.8	2.05	−0.036	2.59	Insoluble	−824.2	0.61 (25)	Circular pits
Cr^{3+}	6.4×10^{-1}	1.44	2.0×10^{-1}	7.2	1.40	−0.71	2.86	Insoluble	–	0.13 (25)	⟨1 1 0⟩ pits

*α_J is calculated taking MgO solubility equal to 8.5×10^{-3} g per 100 cm^3 H_2O.
†Distilled water yields $Mg(OH)_2$ as precipitate.
‡Contrast of pits indicated that $v_t = 3$–$4\ v_n$.
§cw means cold water.
‖Saturated salt solution.

With reference to Table III and Figs 6 and 7, it is easy to see that the apparent rate of lateral growth of dislocation etch pits, v_t', also depends on solution pH, stability of complexes and standard electrode potential of the metal of the impurity cation. The apparent rate of pit deepening, v_n', does not appear to be a simple function of pH, stability of complexes or metal electrode potential.

The standard electrode potentials of metals of additive cations are plotted against the ratio v_t'/v_n' in Fig. 11. From the figure three types of relationship between E^0 and v_t'/v_n' may be identified. In the first category are included Cu, Pb and Cr for which the ratio increases (i.e. the pit contrast decreases) with a decrease in E^0. The ratio v_t'/v_n' is also connected with the equilibrium constant K in this case. In the second category are included Fe, Ni, Co, Cd, Zn and Al. Here the ratio v_t'/v_n' increases with a decrease in E^0, but does not appear to depend on K. In the third category are included Ba and Sr for which the ratio v_t'/v_n' does not depend on E^0.

In comparison with water, the dissolution rate of MgO is fairly increased in aqueous solutions of all salts other than Ba, Sr and Ca. This is anticipated because the value of E^0 for Ba, Sr and Ca is smaller than that for Mg.

The probable factors likely to influence v_d, v_t' and v_n' are essentially the same. Therefore we discuss the formation of dislocation etch pits in terms of crystal solubility. In the crystal growth theories it is realized that the physical properties of the crystal–medium interface determine the growth mechanism. A measure of the nature of the interface is the so-called Jackson surface entropy factor, α_J, defined by [35–37]:

$$\alpha_J = \xi(1 - x_{s,eq})^2(-\ln x_{s,eq} + \Delta f_{sf}) \quad (3)$$

where ξ is the ratio of the slice energy, E_{hkl}^{slice}, of a two-dimensional slice of the thickness of the interplanar distance of the crystallographic face $(h\,k\,l)$ under consideration and the crystallization energy, E^{cr}; $x_{s,eq}$ the ratio of the solute to the solid density and Δf_{sf} the difference in free energy in solid and solute particles. E_{hkl}^{slice} and E^{cr} are obtained from the Hartman–Perdok theory of crystal morphology [38] and Δf_{sf} assumes values between 1 and 2.5 [37].

Computer simulation of growing surface shows that for $\alpha_J < 3.5$ the surface is inherently rough and continuous growth takes place without two-dimensional nucleation, while for $\alpha_J > 3.5$ the surface is smooth and growth is possible only by spiral growth or by two-dimensional nucleation [35–37]. Since the value of $x_{s,eq}$ is altered by selecting different solvents or additives, α_J, and hence the growth mechanism, is directly related with the crystal solubility. The higher the crystal solubility in a medium, the lower is the value of α_J.

There are observations [23–26] that show that the formation of contrasting etch pits is associated with crystal solubility and that surface orientation effects on etch pit formation are suppressed by fast etchants. However, there are few reports [24] that attempt to correlate etch pit formation with α_J. In fact this approach is useful in knowing whether screw dislocation etch pits are formed by a reverse mechanism of spiral growth.

In order to calculate α_J, it is necessary to know ξ, Δf_{sf} and $x_{s,eq}$. For the {1 0 0} face of MgO, $\xi = 1/2$. Since $1 < \Delta f_{sf} < 2.5$, its absolute value will not affect the trend of the curves of α_J versus salt concentration. Therefore we take $\Delta f_{sf} = 1$. The curves of $x_{s,eq}$ can be calculated from solubility data. However, there is a lack of solubility data of MgO in different systems such as the ones employed in this study. Therefore we computed solubility using the experimental values of macroscopic dissolution rates in different solutions, assuming *a priori* that the macroscopic dissolution rate is directly proportional to the crystal solubility.*

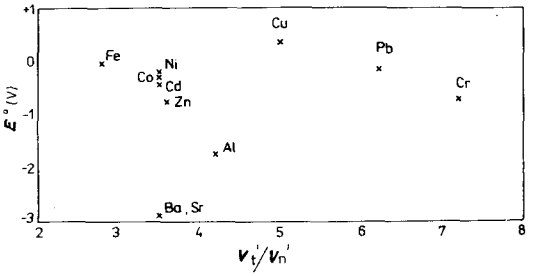

Figure 11 Graph of E^0 versus v_t'/v_n' for 0.5 M solutions of different salts.

*It is not a good approximation to calculate α_J from v_t or v_n data. This is because the chemical nature of a cation and the chemical composition of its complexes are likely to influence the values of v_n more effectively by virtue of different adsorption potentials, thereby altering the rate of two-dimensional nucleation along the dislocation line or the values of v_t by decreasing the kinetics of lateral growth by virtue of their different inhibition capabilities.

The graphs of the dependence of surface entropy factor, α_J, on the concentration of $CuCl_2 \cdot 2H_2O$ and $FeCl_3 \cdot 6H_2O$ are shown in Fig. 12. Since the literature [33] gives two values of the solubility of MgO as 0.00062 and 0.0085 g per 100 cm^3 H_2O at 20 and 30° C respectively, for each salt two α_J versus salt concentration curves are shown in the figure. Except for the absolute values of α_J below which poor etch pits are formed by concentrated $CuCl_2 \cdot 2H_2O$ solutions, the general conclusions are not affected whether we consider the lower or the higher solubility. In the following discussion, however, we take into consideration the higher solubility because for $CuCl_2 \cdot 2H_2O$ this gives a value of $\alpha_J = 3.85$, below which poor pits are formed at screw dislocations. This value of α_J is close to the value formed during computer simulation.

It may be noted from Table III and from Figs 3c and 10b that poorly contrasting pits at screw dislocations are formed by solutions which correspond to a smaller α_J. Exceptions to this generalization are $FeCl_3 \cdot 6H_2O$ and $AlCl_3 \cdot 6H_2O$. The contrast of pits at edge dislocations is maintained in all solutions. The difference in the etching behaviour of edge and screw dislocations at α_J less than about four can therefore be attributed to a difference in the mechanism of etch pit formation at edge and screw dislocations. Since

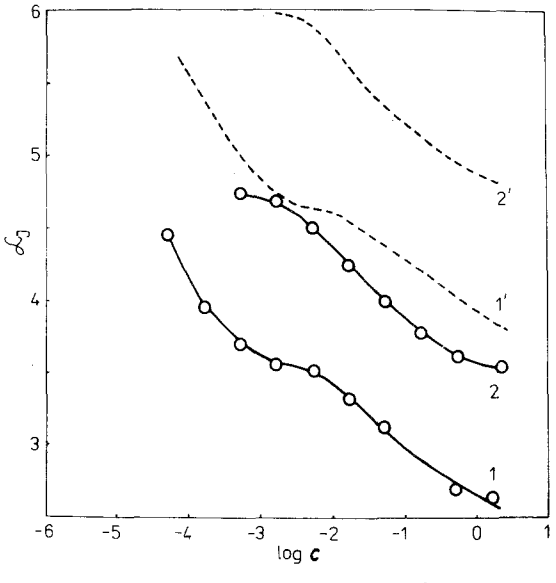

Figure 12 Dependence of surface entropy factor, α_J, on the concentration, c, of (1,1') $FeCl_3 \cdot 6H_2O$ and (2,2') $CuCl_2 \cdot 2H_2O$. Curves 1 and 2, and 1' and 2' correspond to MgO solubility in water equal to 8.5×10^{-3} and 6.2×10^{-4} g per 100 cm^3, respectively.

the parameters that affect v_d and v_t' are the same, we may infer that macroscopic dissolution and lateral etching at dislocations essentially involve two-dimensional nucleation. The contrast of etch pits at edge dislocations is fairly maintained for almost all solutions. This implies that for all values of α_J the normal etching at edge dislocations also takes place by two-dimensional nucleation. A difference in the etching behaviour of screw dislocations in some solutions below and above $\alpha_J \approx 4$ may be explained by considering a transition in the mechanism of etch pit formation. For $\alpha_J > 4$ when the etch pits formed at screw dislocations are contrasting, pit formation takes place by two-dimensional nucleation. For $\alpha_J < 4$ when the screw dislocation pits are poorly revealed, pit formation occurs by a mechanism the reverse of sprial growth.

4.2. Kinetics of dissolution

The dissolution of MgO in water leads to the formation of $Mg(OH)_2$ [39], which may be expressed by the equation

$$MgO + H^+ + OH^- \rightarrow Mg(OH)_2 . \qquad (4)$$

In the presence of a salt which ultimately produces complexes by its dissociation in water according to the typical equations:

$$\begin{aligned} CuCl_2 &\rightarrow 1/n[CuCl_2]_n , \\ CuCl_2 + 5/3\ H_2O &\rightarrow 1/3[CuCl_4]^{2-} \\ &\quad + 2/3[CuCl(H_2O)_5]^+ , \\ CuCl_2 + 4H_2O &\rightarrow [CuCl_2(H_2O)_4] , \\ CuCl_2 + 6H_2O &\rightarrow [Cu(H_2O)_6]^{2+} + 2Cl^- , \end{aligned} \qquad (5)$$

dissolution may be conceived to be accelerated because of the affinity of the complexes to the crystal–etchant interface. The acceleration in dissolution rate depends on the standard electrode potential of the metal of the impurity cation, while the cause of the affinity of complexes to the interface is the adsorption of the OH^- ions from the aqueous solution on to the crystal surface because of the polarizability and rearrangement of the ions composing the surface layer [40]. The reaction at the surface in the presence of a complex may be represented by the following typical equation:

$$\begin{aligned} MgO + [Cu(H_2O)_6]^{2+} + 2OH^- &\rightarrow Mg(OH)_2 \\ &\quad + Cu(OH)_2 + 5H_2O . \end{aligned} \qquad (6)$$

While the electrode potential of the metal of the impurity cation is bound to accelerate dissolution at all salt concentrations, a pronounced acceleration is expected only at those salt concentrations where the complex is positively charged. The experimental results presented above are consistent with this mechanism of impurity action.

The temperature dependence of v_d, v_t' and v_n' for $FeCl_3 \cdot 6H_2O$ (Fig. 8) indicates the same two-dimensional nucleation mechanism for macroscopic, lateral and normal etching throughout the temperature mechanism. For $CuCl_2 \cdot 2H_2O$ (Fig. 9) while macroscopic and lateral etching takes place by two-dimensional nucleation, normal etching at screw dislocations proceeds by two-dimensional nucleation above about 40° C. Below 40° C, normal etching at screw dislocations takes place by a spiral dissolution mechanism. These features may also be noted from the values of activation energies of macroscopic dissolution and apparent lateral and normal etching (Table II). For two-dimensional nucleation $E_d \leqslant E_n'$, but for spiral dissolution mechanism $E_d > E_n'$. However, $E_t' > E_d$ for both two-dimensional nucleation and spiral dissolution mechanisms, for the true selective etching, although $E_t > E_d$, from the absolute values of E_n it is impossible to know to which mechanism it corresponds.

The values of activation energies for macroscopic dissolution, and lateral and normal etching are much greater than the activation energy for diffusion-controlled processes. This means that the dissolution of MgO in aqueous solutions is reaction-rate controlled. It was reported [13, 14] that dissolution of MgO in dilute solutions of acids is reaction-rate controlled, and that the values of E_d and E_t in HCl, HNO_3 and dilute H_2SO_4 are practically the same. This implies that the dissolution of MgO in acids and in inorganic salt solutions is not only reaction-rate controlled, but the absolute values of E_d and E_t are not changed by the presence of a salt or its complexes in solution.

4.3. Morphology of dislocation etch pits

In the light of the morphology of etch pits formed by water (Fig. 2), aqueous solutions of $FeCl_3 \cdot 6H_2O$ of different concentrations (Fig. 4) and aqueous solutions of acids such as HCl, HNO_3 and H_2SO_4 at different concentrations (see [9]), the following sequence of the change of etch pit morphology can be constructed for the {1 0 0} face of MgO crystals: ⟨1 0 0⟩, octagonal, ⟨1 1 0⟩, circular and ⟨1 0 0⟩. With an increase in salt or acid concentration, the first four morphologies are observed in the case of $FeCl_3 \cdot 6H_2O$, the first two in the case of $CuCl_2 \cdot 2H_2O$ and the last three in the case of acids. With a change in additive concentration a similar sequence of the change in pit morphology is found on the {1 0 0} faces of NaCl [41, 42] and CsI crystals [43, 44]. According to the nomenclature used by Hari Babu and Bansigir [41], the first and the last three stages correspond to positive and negative cycles, respectively.

In the case of MgO, two factors that can lead to a change in the pit morphology can be visualized: (a) the solubility of the crystal in a solution and (b) the stability of the complexes. In slow etchants, pits corresponding to one of the stages of the positive cycle, and in fast etchants, pits corresponding to one of the stages of the negative cycle, are formed (see Table III). The main cause for this observation is the solution pH (see Section 4.1). To identify the effect of complexes, we refer to Fig. 1 showing the dependence of pH on salt concentration. At pH = 3.5, the pits formed by $FeCl_3 \cdot 6H_2O$ and $CuCl_2 \cdot 2H_2O$ have ⟨1 1 0⟩ and octagonal morphologies, respectively. Similarly, at pH = 4.5, the pits formed by $FeCl_3 \cdot 6H_2O$ and $CuCl_2 \cdot 2H_2O$ have different and ⟨1 0 0⟩ orientations, respectively. Since Fe and Cu are noble metals, the difference in pit morphology by the two salts can be attributed to a difference in the stability of the complexes of the two salts. A complex with a higher value of K has a poorer tendency to change the pit morphology. This is logical because for a salt ML_n (where M is a metal and L a ligand) which dissociates into ML_{n-1}, the equilibrium constant

$$K_n = \frac{[ML_n]}{[ML_{n-1}]\,[L]}$$

indicates that the inhibiting entity ML_{n-1} is poorly effective for large values of K. A complex that can more easily interact with the lattice ions is more effective in slowing down the motion of dissolution kinks and the criterion for the effectiveness of a complex ML_{n-1} is the stability (or equilibrium) constant of the substituted complex ML_n.

The morphology of etch pits on the {1 0 0} face of MgO, as deduced from the arrangement of ions composing the surface [19] or from periodic bond chain vectors [8, 38], is expected to be ⟨1 0 0⟩.

This morphology is possible only when the rate of sweeping of kinks, q_{sw}, across the dissolution ledges forming at the dislocation site is greater than the rate of their nucleation, q_{nucl}. The rate of kink nucleation increases (i.e. α_J decreases) with an increase in crystal solubility, while the rate of motion of kinks depends on the inhibition mechanism. These two rates ultimately determine the pit morphology [45]. The conditions for the formation of ⟨1 0 0⟩ and ⟨1 1 0⟩ pits are as follows:

$$q_{sw}/q_{nucl} > 1, \quad \langle 1\,0\,0\rangle \text{ pits};$$
$$q_{sw}/q_{nucl} < 1, \quad \langle 1\,1\,0\rangle \text{ pits}.$$

For a discussion of the possible sites for inhibition and the mechanism of inhibition by complexes, the reader is referred to the recent papers [25, 26].

With an increase in the temperature of an etchant containing a particular amount of the additive, the rate of kink nucleation, q_{nucl}, is increased because of an increased crystal solubility, while the rate of sweeping of kinks, q_{sw}, is decreased when the chemical constitution of the complex in solution remains the same or it is increased when the constitution of the complex is changed. This leads to a change in the ratio q_{sw}/q_{nucl} and hence to a change in pit morphology.

4.4. Etch pits at fresh and aged dislocations

All etching solutions employed in the present study form shallower and smaller etch pits at aged dislocations than at fresh ones. $FeCl_3 \cdot 6H_2O$ at low concentrations even forms etch pits of different morphologies on the same surface (Fig. 3a). All etching solutions, without exception, produce shallower and smaller etch pits at screw dislocations than at edge dislocations.

Core and elastic strain energies of screw dislocations emerging at crystal surfaces are somewhat (about 15%) smaller than those of edge dislocations [7, 46]. Also, the dislocation energies of aged dislocations are decreased by impurity segregation at them. Consequently, the formation of shallower etch pits at aged dislocations or at screw dislocations can be attributed to the differences in the dislocation energies. The difference in the morphology of etch pits at fresh and aged dislocations may also be explained from a consideration of the amount and nature of segregated impurities (i.e. dislocation energy). A difference in the size of etch pits at fresh and aged, and at edge and screw dislocations can be explained if two-dimensional surface nucleation is taken into consideration [7, 47].

5. Conclusions

(a) Dissolution rates of {1 0 0} faces of MgO mainly depend on the solution pH, but they are also affected by the standard electrode potential of the metal of the impurity cation and by the stability of the complexes present in solution.

(b) Macroscopic dissolution and lateral growth of etch pits and normal etching along edge dislocation lines occur by two-dimensional nucleation mechanism. In the case of some solutions, normal etching along the screw dislocation lines takes place by two-dimensional nucleation for $\alpha_J > 4$ and by spiral dissolution mechanism for $\alpha_J < 4$.

(c) For two-dimensional nucleation $E_d \leqslant E'_n$, but for spiral dissolution mechanism $E_d > E'_n$. For both two-dimensional nucleation and spiral dissolution mechanisms, $E'_t > E_d$. For the true selective etching of the surface although $E_t > E_d$, from the absolute values of E_n, it is not possible to know to which mechanism it corresponds.

(d) The dissolution of MgO in aqueous acidic salt solutions is reaction-rate controlled. The values of E_d and E_t computed for salt solutions are essentially the same reported for HNO_3, HCl and dilute H_2SO_4. This implies that the absolute values of activation energies are not changed by the presence of salts or complexes in solution.

(e) The morphology of dislocation etch pits depends on (i) the solubility of the crystal in a solution and (ii) the stability of the complexes present in solution.

(f) The formation of shallower etch pits at aged dislocations than at fresh ones or at screw dislocations than at edges is associated with the differences in their dislocation energies. A difference in the morphology of etch pits at fresh and aged dislocations is a consequence of the amount and nature of segregated impurities, while a difference in the size of etch pits at edge and screw and at fresh and aged dislocations is explicable from a consideration of two-dimensional surface nucleation.

Acknowledgements

The author expresses his sincere gratitude to Dr J. Karniewicz, Director of the Institute, for his interest in the work, to Mrs B. Borecka, Dr T. Feliksiński and Mrs B. Wiktorowska for their assistance with the experiments data, and to Dr S. Wysocki for the crystals.

References

1. K. SANGWAL, *J. Mater. Sci.* **15** (1980) 237.
2. N. CABRERA and M. M. LEVINE, *Phil. Mag.* **1** (1956) 450.
3. N. CABRERA, *J. Chim. Phys.* **53** (1956) 675.
4. W. SCHAARWÄCHTER, *Phys. Stat. Solidi* **12** (1965) 375.
5. *Idem, ibid.* **12** (1965) 865.
6. W. K. BURTON, N. CABRERA and F. C. FRANK, *Phil. Trans. Roy. Soc.* **A243** (1951) 299.
7. W. G. JOHNSTON, in "Progress in Ceramic Sciences" Vol. 2, edited by J. E. Burke (Pergamon Press, New York, 1962) p. 1.
8. R. B. HEIMANN, "Auflösung von Kristallen: Theorie und technische Anwendung" (Springer-Verlag, Wien, New York, 1975).
9. K. SANGWAL and J. N. SUTARIA, *J. Mater. Sci.* **11** (1976) 2271.
10. K. SANGWAL and T. C. PATEL, *Krist. Tech.* **13** (1978) 1407.
11. K. SANGWAL, T. C. PATEL and M. D. KOTAK, *ibid.* **14** (1979) 949.
12. *Idem, J. Mater. Sci.* **14** (1979) 1509.
13. *Idem, ibid.* **14** (1979) 1869.
14. K. SANGWAL and S. K. ARORA, *ibid.* **13** (1978) 1977.
15. E. M. NADGORNYI, *Fiz. Tverd. Tela* **5** (1963) 2723.
16. J. J. GILMAN, W. G. JOHNSTON and G. W. SEARS, *J. Appl. Phys.* **29** (1958) 747.
17. A. R. PATEL and J. KOSHY, *Canad. Mineral* **9** (1968) 539.
18. A. R. PATEL and S. K. ARORA, *J. Phys. D: Appl. Phys.* **7** (1974) 2301.
19. M. S. JOSHI and M. A. ITTYACHEN, *J. Appl. Phys.* **40** (1969) 421; *Ind. J. Pure Appl. Phys.* **7** (1969) 624.
20. A. R. PATEL and O. P. BAHL, *Brit. J. Appl. Phys.* **16** (1966) 169.
21. A. R. PATEL and R. M. CHAUDHRI, *Jap. J. Appl. Phys.* **8** (1969) 677.
22. A. R. PATEL and B. P. AGARWAL, *J. Phys. D: Appl. Phys.* **4** (1971) 985.
23. B. JESZENSZKY, *Nature* **181** (1958) 559.
24. K. SANGWAL, M. SZURGOT, J. KARNIEWICZ and W. KOLASINSKI, *J. Crystal Growth* **58** (1982) 261.
25. K. SANGWAL, *J. Mater. Sci.*, in press.
26. K. SANGWAL and A. A. URUSOVSKAYA, *Prog. Cryst. Growth Character* in press.
27. N. N. GREENWOOD, E. J. F. ROSS and B. P. STRAUGHAN, "Index of Vibration Spectra of Inorganic and Organometallic Compounds", Vol. 1 (Butterworths, London, 1964).
28. C. K. JÖRGENSEN, "Inorganic Complexes" (Academic Press, London, 1963).
29. H. D. LUEDEMAN and E. U. FRANCK, *Ber. Bunsenges. Phys. Chem.* **71** (1967) 455.
30. S. N. ANDREEV and O. V. SAPOZHNIKOVA, *Zh. Neorg. Khimii* **10** (1965) 2538; **13** (1968) 1548.
31. I. I. ANTIPOVA-KARATAEVA, Yu. A. ZOLOTOV and I. V. SERYAKOVA, *ibid.* **9** (1964) 1712.
32. K. SANGWAL, N. L. SIZOVA and A. A. URUSOVSKAYA, *Krist. Tech.* **12** (1977) 567.
33. I. GAJEWSKA, S. PIETRAS, J. RUDZIŃSKA and A. SCHELLENBERG (eds), "Poradnik Fizykochemiczny" (Physico-chemical Handbook) (Naukowotechniczne press, Warsaw, 1974).
34. J. BJERRUM, G. SCHWARZENBACH and L. G. SINLÉN, "Stability Constants, Part 2: Inorganic Ligands" (Chemical Society, London, 1958).
35. P. BENNEMA, in "Industrial Crystallization 78", edited by E. J. De Jong and S. J. Jančić (North-Holland, Amsterdam, 1979) p. 115.
36. H. J. HUMAN, J. P. VAN DER EERDEN, L. A. M. J. JETTEN and J. G. M. ODEKERKEN, *J. Crystal Growth* **51** (1981) 589.
37. P. BENNEMA and J. P. VAN DER EERDEN, *ibid.* **42** (1977) 201.
38. P. HARTMAN, in "Crystal Growth: an Introduction", edited by P. Hartman (North-Holland, Amsterdam, 1973) p. 363.
39. J. GAŁECKI, "Preparatyka Nieorganiczna" (Practical Inorganic Chemistry) (Naukowo-techniczne Press, Warsaw, 1964) p. 2423.
40. W. A. WEYL, in "Structure and Properties of Solid Surfaces" edited by R. Gomer and C. S. Smith (University of Chicago Press, Chicago, 1953) p. 147.
41. V. HARI BABU and K. G. BANSIGIR, *J. Phys. Soc. Japan* **23** (1967) 860.
42. *Idem, J. Crystal Growth* **2** (1968) 9.
43. K. SANGWAL and A. A. URUSOVSKAYA, *ibid.* **41** (1977) 216.
44. K. SANGWAL, A. A. URUSOVSKAYA and A. E. SMIRNOV, *Ind. J. Pure Appl. Phys.* **16** (1978) 501.
45. M. B. IVES, *J. Phys. Chem. Solids* **24** (1963) 275.
46. H. B. HUNTINGTON, J. E. DICKEY and R. THOMSON, *Phys. Rev.* **100** (1955) 1117.
47. J. D. LIVINGSTON, in "Direct Observation of Imperfections in Crystals" edited by J. B. Newkirk and J. H. Wernick (John Wiley, New York, London, 1962) p. 115.

Received 26 April and accepted 24 May 1982